DOI 10.1007/s11204-015-9309-9
Soil Mechanics and Foundation Engineering, Vol. 52, No. 2, May, 2015 (Russian Original No. 2, March-April, 2015)

NUMERICAL MODELLING OF HYDRAULIC FRACTURING IN ROCK MASS BY XFEM

UDC 518.5/539.388.8

Luyang Shi,[1] Tiantang Yu,[1] and Tinh Quoc Bui[2]
[1]Hohai University, Nanjing, China;
[2]Tokyo Institute of Technology, Ookayama, Meguro-ku, Tokyo, Japan.

A numerical model based on the extended finite element method (XFEM) is developed to serve this purpose. The present approach involves several features of an effective numerical tool in modelling hydraulic fracturing: the generalized shape functions are used in a cluster of nodes around the cracks, whereas the conventional finite element shape functions are applied outside the cracks; the ramp function is introduced to remove the blending elements in the XFEM setting; and the contact conditions between crack faces are considered by combining the mortar method with the augmented Lagrange's method. This study assumes uniform water pressures at the crack faces. The effect of the water pressure on the fracture behaviours of cracks and the interaction between the hydraulic and natural fractures are analyzed. Numerical examples are presented and discussed to show that the water pressure acting on the crack faces has a significant influence on the stress and the deformation in the vicinity of the cracks, and the crack propagation path depends on the mechanical properties of rock mass and natural fracture faces, water pressure, in-situ stresses, and relative positions of natural and hydraulic fractures.

1. Introduction

Hydraulic fracturing is the fracturing of porous media, such as rock, soil or concrete, by a pressurised liquid, and was first used to increase production in the oil and gas industry. Hydraulic fracturing has been widely used in many engineering applications, including measuring in-situ stresses [1], stimulating groundwater wells [2], increasing injection rates for hazardous solid waste disposal [3] and enhancing hydrocarbon production and geothermal energy extraction [4]. However, hydraulic fracturing sometimes may cause severe disasters in engineering. The Malpasset dam in France [5] and the Teton dam in the USA [6] are typical engineering accidents caused by hydraulic fracturing. Thus, hydraulic fracturing in rock mass has become a concern in rock engineering.

Natural fractures are present in rock mass, so the interaction between hydraulic and natural fractures is required in the analysis of hydraulic fracturing of rock mass. Given its complexity, research on the interaction between the natural and hydraulic fractures has focused on experimental tests [7] and numerical simulation. Several numerical methods have been proposed to solve hydraulic fracturing problems, including the finite element method (FEM) [8], boundary element method (BEM) [9], element-free method[10], and finite difference method [11]. However, the mesh must be aligned with the crack path

Translated from Osnovaniya, Fundamenty i Mekhanika Gruntov, No. 2, p. 12, March-April, 2015.
0038-0741/15/5202-0074

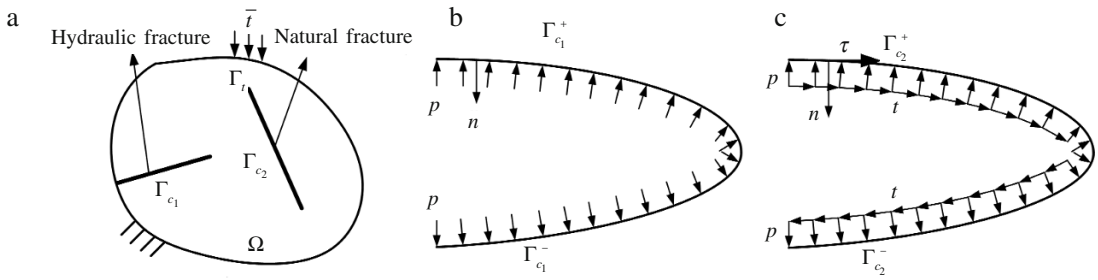

Fig.1. Schematic description of tractions acting on the fracture faces: the rock mass containing a natural fracture and hydraulic fracture (a); the water pressure on the hydraulic fracture faces (b); and the contact forces on the natural fracture faces (c).

in FEM and BEM, and a re-meshing technique is required for the methods as the crack propagates. Although the element-free method can conveniently deal with crack propagation problems, their computational costs are high to model multiple cracks.

To overcome the inherent drawbacks associated with the use of FEM and BEM in the simulation of fracture propagation problems, Belytschko and co-worker [12] proposed the extended finite element method (XFEM). Numerous studies have been conducted to improve and/or apply XFEM to model fracture propagation problems, including hydraulic fracture problems. Lecampion [13] modelled the fluid pressure and fracture opening in hydraulic fracture using XFEM for the behaviours of two limiting tips in the impermeable case.

To improve the accuracy of values in the vicinity of cracks, the first-order generalized node shape functions are used at the nodes around the cracks, whereas the conventional finite element shape functions are adopted at nodes outside the cracks. The ramp function is used to remove the blending elements, and the junction enrichment function is used to model the crack junction. A combination of the mortar method (i.e., segment-to-segment contact approach) with the augmented Lagrange's method is adopted to establish the contact between natural fracture faces. In this work, the water pressure on the crack faces is considered as a constant, i.e., the uncoupled hydraulic fracturing model is applied.

This paper is organized as follows. Section 2 presents the governing equations of hydraulic fracturing in rock mass. Section 3 presents the XFEM formulation for hydraulic fracturing in rock mass. Section 4 presents the crack propagation. Numerical validation is studied in Section 5, while Section 6 presents our numerical applications using the present XFEM method. We will end with concluding remarks in the last section.

2. Governing equations of hydraulic fracturing in rock mass

Consider a two-dimensional rock mass domain Ω containing a natural fracture and hydraulic fracture, as depicted in Fig. 1, a. The boundary of the domain Γ is composed of the stress boundary Γ_t, displacement boundary Γ_u and crack face Γ_c. The crack face contains both the hydraulic fracture face Γ_{c_1} and natural fracture face Γ_{c_2}, i.e., $\Gamma = \Gamma_t \cup \Gamma_u \cup \Gamma_{c_1} \cup \Gamma_{c_2}$. The water pressures are applied on the hydraulic fracture faces. The water pressure on the hydraulic fracture faces may cause the natural fracture faces to close, so the contact forces on the natural fracture faces must be considered. For simplicity, we do not distinguish the water pressures on hydraulic fracture faces and the contact forces on natural fracture faces, both of which are denoted as $\overline{\overline{t}}$. However, we distinguish the crack faces Γ_c^+ and Γ_c^- as shown in Fig. 1, b, c, so that $\Gamma_c = \Gamma_c^+ \cup \Gamma_c^-$. The tractions $\overline{\overline{t}}$ and $-\overline{\overline{t}}$ are imposed on Γ_c^+ and Γ_c^-, respectively.

The equilibrium equations and boundary conditions are

$$\nabla\sigma + b = 0 \text{ in } \Omega \tag{1}$$

$$\sigma n = \bar{t} \text{ on } \Gamma_t \tag{2}$$

$$u = \bar{u} \text{ on } \Gamma_u \tag{3}$$

$$\sigma n = \bar{\bar{t}} \text{ on } \Gamma_{c_1}^{+} \cup \Gamma_{c_2}^{+} \tag{4}$$

$$\sigma(-n) = -\bar{\bar{t}} \text{ on } \Gamma_{c_1}^{-} \cup \Gamma_{c_2}^{-}, \tag{5}$$

where σ is the Cauchy stress tensor, b is the body force, $\bar{t}$ is the prescribed external traction on Γ_t, u is the displacement, $\bar{u}$ is the prescribed displacement on Γ_u, and n is the outward unit normal vector on Γ_t and Γ_c^{+}.

During the hydraulic fracturing process, contact between the two crack faces of natural fracture may occur. To consider the mechanical behaviour of the natural fracture, the contact conditions between crack faces must be considered. The augmented Lagrange's multipliers are introduced between the crack faces, which are expressed as

$$\overline{\lambda_n} = \lambda_n + E_n u_n, \ \overline{\lambda_\tau} = \lambda_\tau + E_\tau u_\tau, \tag{6}$$

where λ_n and λ_τ are the normal and tangential Lagrange's multipliers, and E_n and E_τ are the normal and tangential penalty factors, respectively. The relative displacements in normal and tangential directions of any pair of contact points are

$$u_n = u_n^{+} - u_n^{-}, \ u_\tau = u_\tau^{+} - u_\tau^{-}, \tag{7}$$

where (u_n^{+}, u_τ^{+}) and (u_n^{-}, u_τ^{-}) are the normal and tangential displacements of any pair of contact points on $\Gamma_{c_2}^{+}$ and $\Gamma_{c_2}^{-}$, as in Fig. 1, c.

Generally, the interpolation of the augmented Lagrange's multipliers field can be expressed as

$$\overline{\lambda}_j^h = \sum_{i=1}^{2} M_i(x)\overline{\lambda}_{ji} \quad (j = n, \tau), \tag{8}$$

where $M_1(\zeta) = (1 - \zeta)/2$, $M_2(\zeta) = (1 + \zeta)/2$, ζ is the local coordinate along the crack, and $\overline{\lambda}_{ji}$ is the value at the crack-mesh intersection or inflection point of the crack.

So the weak form of the equilibrium equation is

$$\int_\Omega \frac{\varepsilon(v)}{\sigma(u)} d\Omega + \int_{\Gamma_{c_2}^{+}} \bar{\bar{t}}\, v^{+} dS - \int_{\Gamma_{c_2}^{-}} \bar{\bar{t}}\, v^{-} dS = \int_\Omega bv d\Omega + \int_{\Gamma_t} \bar{t} v dS + \int_{\Gamma_{c_1}^{+}} \bar{\bar{t}}\, v^{+} dS - \int_{\Gamma_{c_1}^{-}} \bar{\bar{t}} v^{-} dS, \tag{9}$$

where u is the trial function that satisfy all displacement boundary conditions and usual smoothness $C^0(\Omega)$, v is the test function, v^{+} and v^{-} are the virtual displacements on $\Gamma_{c_1}^{+}$ and $\Gamma_{c_1}^{-}$.

By setting $u_c = v^{+} - v^{-}$, considering the frictional contact condition between crack faces, we can express the weak form of the equilibrium equation, Eq. (9), as

$$\int_\Omega \frac{\varepsilon(v)}{\sigma(u)} d\Omega + \int_{\Gamma_{c_2}} (\overline{\lambda}_n^h \delta u_n + \overline{\lambda}_\tau^h \delta u_\tau) dS = \int_\Omega b \cdot \delta u d\Omega + \int_{\Gamma_t} \bar{t} \delta u dS + \int_{\Gamma_{c_1}} \bar{\bar{t}} u_c dS. \tag{10}$$

3. XFEM for hydraulic fracturing in rock mass

In XFEM, the standard displacement approximation around the crack is enriched with the discontinuous step function in the split elements, asymptotic fields near the crack tip, and junction-

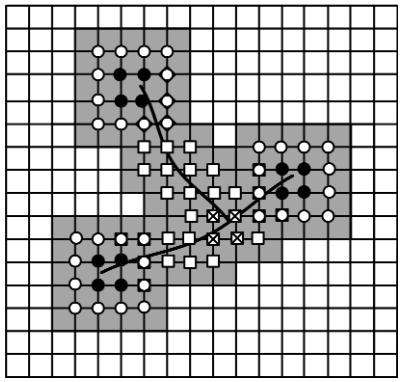

Fig.2. Enriched nodes and enrichment types: □) Nodal set J; ●) Nodal set K^*; ○) Nodal set K; ×) Nodal set L; gray areas show where the nodal generalized shape functions are used.

enriched function in the junction elements. The enriched displacement approximation can be written as follows:

$$u^h(x) = \sum_{i\in I} N_i(x)u_i + \sum_{j\in J} N_j(x)\left(H(x) - H(x_j)\right)a_j + \sum_{\alpha=1}^{4}\sum_{k\in K} N_k(x)\left(F_\alpha(x) - F_\alpha(x_k)\right)R^\alpha(x)b_{k\alpha} + \\ + \sum_{l\in L} N_l(x)\left(J(x) - J(x_l)\right)c_l, \tag{11}$$

where $N_i(x)$ is the finite element shape function; u_i, a_j, $b_{k\alpha}$ and c_l are the displacements and enrichment nodal variables; I is the set of all nodes in the discretisation; J is the set of nodes whose support is entirely split by the crack (the squared nodes in Fig.2) and are enriched with a modified Heaviside step function $H(x)$, which assumes the value +1 above the crack and −1 below the crack; K^* is the set of nodes whose support is partly split by the crack (the circled solid nodes in Fig.2); K is the set of nodes in K^* plus their nearby nodes (the circled hollow nodes in Fig.2) and are enriched with the crack-tip fields; L is the set of nodes whose support contains the junction (the crossed nodes in Fig.2); and $R(x) = \sum_{i\in K^*} N_i(x)$ is the ramp function [14] whose introduction can remove the blending elements.

For an isotropic elastic material, the crack-tip branch enrichment functions $F_a(x)$ (α = 1,…,4) are defined as

$$F_\alpha(r,\theta) = \left[\sqrt{r}\sin\frac{\theta}{2}\sqrt{r}\cos\frac{\theta}{2}\sqrt{r}\sin\frac{\theta}{2}\sin\theta\sqrt{r}\cos\frac{\theta}{2}\sin\theta\right], \tag{12}$$

where r and θ are the local crack tip polar coordinates.

The junction enrichment function $J(x)$ is chosen as [15]:

$$J(x) = \begin{cases} H\left(f_1(x)\right) - H\left(f_1(x_i)\right) & \text{for } f_1(x)f_1(x_i) > 0 \\ H\left(f_2(x)\right) - H\left(f_2(x_i)\right) & \text{for } f_1(x)f_1(x_i) < 0 \end{cases}, \tag{13}$$

where $f_1(x)$ and $f_2(x)$ are the signed distance functions of the master crack (the crack with two crack tips in Fig.2) and minor crack (the crack with one crack tip in Fig.2), respectively.

To improve the accuracy of stresses around the crack at a low cost, $N_i(x)$ around the cracks is adopted as the generalized shape function, whereas the conventional finite element shape function is used outside the crack. In Fig.2, the red domains show where the nodal generalized shape functions are used. Considering the cost and accuracy, the first-order nodal displacement interpolation function is used, and the generalized shape function matrix of node i is expressed as follows [16]:

$$N_i = \varphi_i \begin{bmatrix} 1 & 0 & x-x_i & 0 & y-y_i & 0 \\ 0 & 1 & 0 & x-x_i & 0 & y-y_i \end{bmatrix}, \tag{14}$$

where φ_i is the conventional finite element shape function and $(x_i.\ y_i)$ are the coordinates of node i.

By discretizing Eq. (10) with XFEM, we obtain the governing equation for hydraulic fracturing in the rock mass:

$$(K + K_c)d = f, \tag{15}$$

where $d = [u\ a\ b\ c]^T$ is the array of nodal unknowns, and K, K_c, and f are the global stiffness matrixes, the stiffness matrix on the contact crack faces, and external nodal force vector, respectively.

4. Crack propagation

The stress intensity factors are computed using the interaction integral method. Two scenarios are considered: scenario 1 ($\sigma_{ij}^{(1)}$, $\varepsilon_{ij}^{(1)}$, $u_i^{(1)}$) corresponds to the actual state; scenario 2 ($\sigma_{ij}^{(2)}$, $\varepsilon_{ij}^{(2)}$, $u_i^{(2)}$) is an auxiliary state that will be chosen as the asymptotic fields for model I or II. In the presence of tractions on the crack faces, such as frictional force or water pressure, the interaction integral may be written as follows[17]:

$$I^{(1,2)} = \int_A \left[-W^{(1,2)}\delta_{1j} + \sigma_{ij}^{(1)} \frac{\partial u_i^{(2)}}{\partial x_1} + \sigma_{ij}^{(2)} \frac{\partial u_i^{(1)}}{\partial x_1} \right] \frac{\partial q}{\partial x_j} dA - \int_{C_+ + C_-} \left[\sigma_{i2}^{(1)} \frac{\partial u_i^{(2)}}{\partial x_1} + \sigma_{i2}^{(2)} \frac{\partial u_i^{(1)}}{\partial x_1} \right] q m_2 d\Gamma, \tag{16}$$

where $W^{(1,2)} = \sigma_{ij}^{(1)}\varepsilon_{ij}^{(2)} = \sigma_{ij}^{(2)}\varepsilon_{ij}^{(1)}$ is the interaction strain energy; q is a weighting function, which takes a value of unity on an open set containing the crack tip and vanishes on an outer prescribed contour; m_j is the outward normal to the domain used for the computation of stress intensity factors; and C denotes the hydraulic fracture faces Γ_{c_1} and natural fracture faces Γ_{c_2}, i.e., $C = \Gamma_{c_1} \cup \Gamma_{c_2}$.

By selecting the auxiliary state as the pure mode I or II asymptotic fields, we can obtain the stress intensity factors of modes I and II:

$$K_I^{(1)} = \frac{2}{E^*} I^{(1,\mathrm{mode\ I})},\ K_{II}^{(1)} = \frac{2}{E^*} I^{(1,\mathrm{mode\ II})}, \tag{17}$$

where $E^* = E$ is the plane stress, and $E^* = E/(1 - \nu^2)$ is the plane strain.

The crack growth angle in the local crack-tip coordinate system can be expressed as

$$\theta = 2\tan^{-1}\left(\frac{K_I - \sqrt{(K_I)^2 + 8(K_{II})^2}}{4K_{II}} \right). \tag{18}$$

In Eq. (18), the fracture mode is pure mode I for $K_{II} = 0$; then $\theta = 0$; the crack growth angle $\theta < 0$ when $K_{II} > 0$, and $\theta > 0$ when $K_{II} < 0$.

TABLE 1

Size of the plate		Normalized stress intensity factors obtained by				
b/a	*c/a*	proposed XFEM	standard XFEM	SBFEM [19]	BCM [18]	analytical solution [20]
4	3	1.840	1.839	1.838	1.8384	1.93
8	5	1.274	1.271	1.297	1.2670	1.35
12	7	1.253	1.252	1.254	1.2521	1.26
16	9	1.201	1.198	1.206	1.1979	1.20
20	11	1.199	1.203	1.205	1.1859	1.19
∞	∞	1.1215	1.1215	1.1215	/	1.1215

For the closed natural fracture, a certain anti-tension strength exists on the crack faces. The natural fracture will open when the effective normal stress on the natural fracture faces reaches the anti-tension strength.

5. Numerical validation

To validate the accuracy of the developed XFEM model, an edge-cracked rectangular plate with the height b units and the width c units under water pressure p units acting on the crack faces is analyzed; and the crack length is in a units centred at of the crack height. Young's modulus E is chosen as 1,000 Pa, and Poisson's ratio v is taken as 0.3. In the numerical analysis, the displacement along the vertical direction is fixed at the bottom right corner, and the plate is clamped at the bottom left corner; plane strain conditions are assumed, and the nodes in one layer of elements around the crack have generalized shape functions.

The normalized stress intensity factors with $p\sqrt{\pi a}$ are computed and compared with the standard XFEM, boundary collocation method (BCM) [18], scaled boundary finite element method (SBFEM) [19], and analytical solutions [20], as shown in Table 1. The numerical results obtained by the developed XFEM are shown to be in good agreement with the reference SBFEM, BCM, and analytical solutions, which confirms the higher accuracy of the developed XFEM than the standard XFEM; thus the proposed method can improve the accuracy.

6. Numerical examples

In this section, two numerical examples are presented to assess the robustness of the developed XFEM for simulating the hydraulic fracturing in rock mass. In all examples reported below, Poisson's ratio v is taken as 0.3 and Young's modulus E is chosen as 1,000 MPa, the penalty factors are $E_n = E_\tau = 1{,}000E$, the friction coefficient between crack faces is $\mu = 0.3$, the critical energy release rate of rock mass $G_c = 0.1$ MPa·m, the initial state of natural fracture is closed, and the tensile strength of natural fracture is $f_t = 0.005$ MPa. Plane strain conditions are assumed, and the nodes in one layer of elements around the crack have generalized shape functions.

6.1 One horizontal hydraulic fracture and one oblique natural fracture

One domain, including one horizontal hydraulic fracture and a natural fracture with inclination angle 63.4°, is shown in Fig. 3, a, and the enriched styles are shown in Fig. 3, b. The water pressure inside the hydraulic fracture is $p = 10$ kPa.

The hydraulic fracturing process is simulated in two steps. In each step, the crack propagates a distance of 0.26 m. Table 2 shows the energy release rates (kPa·m) of three crack tips labelled (1), (2) and (3) in Fig. 3, a for each step. The energy release rate of the hydraulic fracture tip is much bigger than those of the two natural fracture tips and bigger than the critical energy release rate. Thus, the hydraulic fracture tip propagates by the direction of maximum hoop stress, whereas the two natural fracture tips stop. When the hydraulic fracture tip intersects with the natural fracture, the crack tip-enriched elements of the hydraulic fracture become the junction-enriched elements.

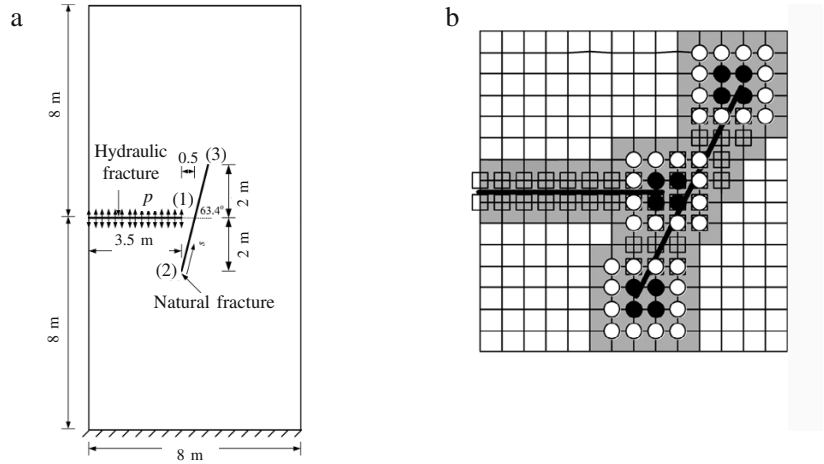

Fig.3. One domain including an oblique natural fracture and one horizontal hydraulic fracture (a); enriched style around the cracks (b).

TABLE 2

Step	Tip (1)	Tip (2)	Tip (3)
0	1,057	11.6	19.6
1	1,849	39.4	51.5
2	3,488	78.2	81.5

Fig.4 shows the opening displacements of the natural fracture during hydraulic fracture propagation. The following features observed from the results may be evident: (1) the part of the natural fracture around the hydraulic fracture tip is under tensile stress due to the water pressure on the hydraulic fracture; (2) in the zone far from the hydraulic fracture tip (around the natural fracture tips) the hydraulic fracture exerts compression on the natural fracture, so the natural fracture faces are closed; (3) the opening displacement is larger when the hydraulic fracture tip is closer to the natural fracture; (4) the natural fracture is asymmetric, so the hydraulic fracture propagates in the direction with smaller pressure (far from the hydraulic fracture).

6.2 One horizontal hydraulic fracture and one oblique natural fracture under far field stress

Similar to the above example, one domain, including one horizontal hydraulic fracture and one oblique natural fracture, under far field stress in parallel and vertical directions σ_∞ = 1 MPa and water pressure p = 1 MPa is considered.

The contact stresses along the natural fracture are shown in Fig.5. Around the hydraulic fracture tip, hydraulic fracturing generates tensile stress to the natural fracture, and the far field stress generates pressure to the natural fracture. The natural fracture around the hydraulic fracture tip is under water pressure because of both hydraulic fracturing and far field stress. In the entire zone of the natural fracture, the normal stress $\overline{\lambda}_n$ and shear stress $\overline{\lambda}_\tau$ satisfy $|\overline{\lambda}_\tau| < \mu|\overline{\lambda}_n|$, so the entire natural fracture is in the adhesive state.

The crack growing process is simulated in four steps. In each step, the crack propagates a distance of 0.26 m. To investigate the effect of the mechanical properties of natural fracture faces on the propagation path, several different mechanical properties of the natural fracture faces are considered.

After the hydraulic fracture intersects with the natural fracture, for the closed natural fracture, if the effective normal stresses σ^e (water pressure plus normal contact stress $\sigma^e = p + \sigma_n$) of the natural

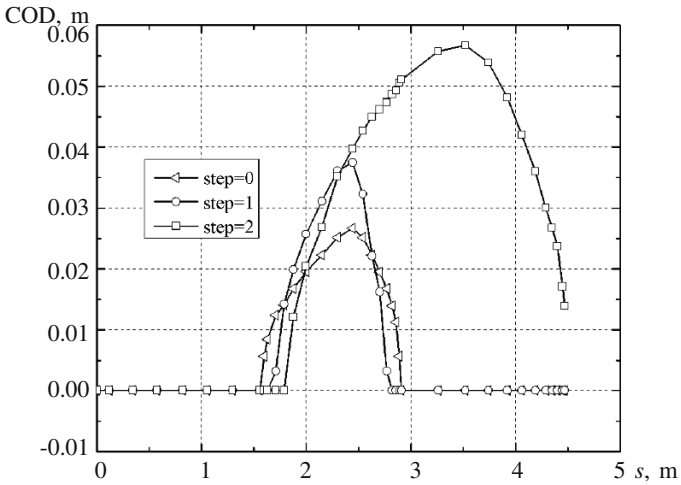

Fig.4. Crack opening displacements along the natural fracture.

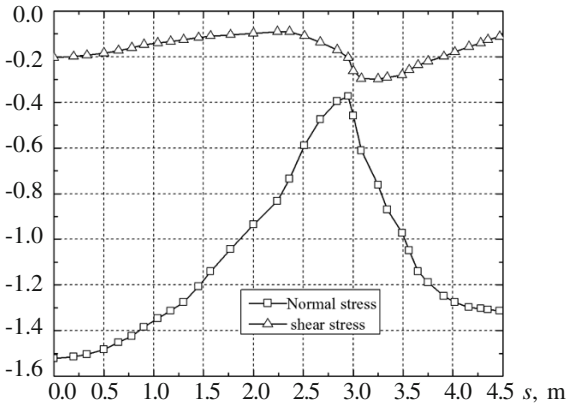

Fig.5. Contact stress along the natural fracture under far field stress.

fracture faces at the present and next hydraulic fracture tips reach the anti-tensile strength, the closed crack faces will open. To investigate the effect of the mechanical properties of the natural fracture faces on the propagation path, three cases are considered. Case (1): The critical energy release rate of the rock mass is G_c^{rock} = 0.05 MPa·m, and the water pressure is p = 0.5 MPa. The normal contact stress at the intersection is −0.61 MPa. When the hydraulic fracture intersects with the natural fracture, the natural fracture may open at the intersection along two directions (i.e., the positive direction of s and the negative direction of s). The normal contact stress at the next hydraulic fracture tip in the positive and negative directions of s is −0.53 and −0.79 MPa, respectively. The effective normal stresses at the present and next hydraulic fracture tips are less than f_t, so the water may not enter the natural fracture. Thus, the hydraulic fracture is arrested by the natural fracture. Case (2): The critical energy release rate of the rock mass is G_c^{rock} = 0.1 MPa·m, and the water pressure is p = 2 MPa. In this case, the normal contact stress at the intersection is −0.09 MPa. When the hydraulic fracture intersects with the natural fracture, the normal contact stresses at the next hydraulic fracture tip in the positive and negative directions of s are −0.03 and −0.10 MPa, respectively. The effective normal stresses at the present and next hydraulic fracture tips in the positive and negative directions of s are greater than f_t, so the hydraulic fracture propagates in the two directions along the closed natural fracture for one step. Thus, the normal contact stresses at the next hydraulic fracture tip in the positive and negative directions of s are −0.13 and −0.22

MPa, respectively. The effective normal stresses at the present and next hydraulic fracture tips in the positive and negative directions of s are greater than f_t, so the hydraulic fracture still propagates in the two directions along the closed natural fracture for one step. Case (3): The critical energy release rate of the rock mass is G_c^{rock} = 0.1 MPa·m, and the water pressure is p = 10 MPa. In this case, the normal contact stress at the intersection is 1.51 MPa. When the hydraulic fracture intersects with the natural fracture, the normal contact stresses at the next hydraulic fracture tip in the positive and negative directions of s are 2.96 and 0.20 MPa, respectively. These normal stresses are greater than f_t, so the hydraulic fracture propagates in the two directions along the closed natural fracture for one step. Thus, the normal contact stresses at the next hydraulic fracture tip in the positive and negative directions of s are 4.59 and –0.17 MPa, respectively. The effective normal stresses at the present and next hydraulic fracture tips in the positive direction of s are greater than f_t, whereas the effective normal stresses at the next hydraulic fracture tip in the negative direction of s is less than f_t, so the hydraulic fracture still propagates in the positive direction along the closed natural fracture for one step.

The results show that the mechanical properties of natural fracture faces and water pressure have a significant effect on the hydraulic fracture propagation.

Conclusion

Based on the uncoupled hydraulic fracturing model, an XFEM model of hydraulic fracturing is developed to investigate the hydraulic fracturing phenomenon in rock mass. To improve the accuracy around the fracture at a low cost, the generalized shape functions are used in a cluster of nodes around the fractures, whereas the conventional finite element shape functions are applied outside the fractures. The ramp function is introduced to remove the blending elements. The mortar method (e.g., segment-to-segment contact approach) is combined with the augmented Lagrange's method to treat the contact conditions between facture faces. The accuracy of the developed XFEM for hydraulic fracturing is very good, as validated by the reference solution. Numerical results show that the water pressure acting on the fracture faces influences significantly the stress and deformation in the vicinity of the fractures, and the fracture propagation path depends on the mechanical properties of rock and natural fracture face, water pressure, in-situ stresses, and relative positions of natural and hydraulic fractures.

Acknowledgements

The financial support by the National Natural Science Foundation of China (Grant No. 51179063) and the Graint-in-Aid for Scientific Research (No. 26-04055), Japan Society for the Promotion of Science (JSPS, ID No. P14055), is gratefully acknowledged.

REFERENCES

1. A.M.Raaen, E.Skomedal, H.Kjorholt, P.Markestad, D.Okland, "Stress determination from hydraulic fracturing tests: the system stiffness approach," *Int. J. Rock Mech. Min. Sci.*, **38**, 529-541(2001).
2. L.C.Murdoch, and W.W.Slack, "Forms of hydraulic fractures in shallow fine-grained formations," *Geotech. Geoenviron. Eng.*, **128**, 479-487(2002).
3. B.W.Hainey, R.G.Keck, M.B.Smith, K.W.Lynch, J.W.Barth, "On-site fracturing disposal of oilfield-waste solids in Wilmington field, Long Beach Unit, CA," *Western regional meeting*, No.67, 25(6), 77-84(1997).
4. S.Sasaki, "Characteristics of microseismic events induced during hydraulic fracturing experiments at the Hijiori hot dry rock geothermal energy site, Yamagata, Japan," *Tectonophysics*, **289**, 171-188 (1998).
5. P.Habib, "The MalPasset dam failure," *Eng. Geol.*, **24**, 331-338 (1987).
6. B.E.Fueik, "The Teton dam failure - a diseussion," *Eng. Geol.*, **24**, 207-215 (1987).
7. J.Zhou, M.Chen, Y.Jin, G.Zhang, "Analysis of fracture propagation behavior and fracture geometry using a tri-axial fracturing system in naturally fractured reservoirs," *Int. J. Rock Mech. Min. Sci.*, **45**, 1143-1152 (2008).
8. B.Carrier, and S.Granet, "Numerical modeling of hydraulic fracture problem in permeable medium using cohesive zone model," *Eng. Fract. Mech.*, **79**, 312-328 (2012).

9. V.Koshelev, and A.Ghassemi, "Hydraulic fracture propagation near a natural discontinuity," *Twenty-Eighth Workshop on Geothermal Reservoir Engineering*, Stanford University, Stanford, California, January 27-29,(2003).
10. R.P.Kumar, and G.R.Dodagoudar, "Modeling of contaminant transport through landfill liners using EFGM," *Int. J. Numer. Anal. Methods Geomech.*, **34**, 661-688 (2010).
11. L.Zhou, and M.Z.Hou, "A new numerical 3D-model for simulation of hydraulic fracturing in consideration of hydro-mechanical coupling effects," Int. J. Rock Mech. Min. Sci., **60**, 370-380 (2013).
12. T.Belytschko, and T.Black, "Elastic crack growth in finite elements with minimal remeshing," *Int. J. Numer. Meth. Eng.*, **45**, 601-620 (1999).
13. B.Lecampion, "An extended finite element method for hydraulic fracture problems," *Commun. Numer. Meth. Eng*., **25**, 121-133 (2009).
14. T.P.Fries, "A corrected XFEM approximation without problems in blending elements," *Int. J. Numer. Meth. Eng.*, **75**, 503-532 (2008).
15. È .Budyn, N.Moë s, T.Belytschko, "A method for multiple crack growth in brittle materials without remeshing," *Int. J. Numer. Meth. Eng.*, **61**, 1741-1770 (2004).
16. T.T.Yu, and P.Liu, "Improved implementation of the extended finite element method for stress analysis around cracks," *Archives of Civil and Mechanical Engineering*, **XI**, 787-805 (2011).
17. J.Dolbow, N.Moë s, T.Belytschko, "An extended finite element method for modeling crack growth with frictional contact," *Comp. Meth. Appl. Mech. Eng*., **190**, 6825-6846 (2001).
18. C.L.Tu, "The boundary collocation method and it s application to crack surface under external force," *Hydraul. Eng*. (in Chinese), **7**, 9-16 (1983).
19. J.Y.Liu, "Effect of the Water Pressure inside the Crack on the Fracture Behavior of Concrete Gravity Dam," *Dalian University of Technology* (in Chinese), China (2008).
20. H.Tada, P.C.Paris, R.Irwin, *The stress analysis of cracks Handbook*, Del Research Corporation, Hellertown, Pennsylvania (1973).